

Diversity of Fuzzy Dark Matter Solitons

Chen Tan^{1,2,3,4} and Ke Wang^{1,2,3,4*}

¹*School of Physical Science and Technology, Lanzhou University, Lanzhou 730000, China*

²*Institute of Theoretical Physics & Research Center of Gravitation, Lanzhou University, Lanzhou 730000, China*

³*Key Laboratory of Quantum Theory and Applications of MoE,
Lanzhou University, Lanzhou 730000, China and*

⁴*Lanzhou Center for Theoretical Physics & Key Laboratory of Theoretical
Physics of Gansu Province, Lanzhou University, Lanzhou 730000, China*

(Dated: November 26, 2024)

According to the Schrödinger-Poisson equations, fuzzy dark matter (FDM) can form a stable equilibrium configuration, the so-called FDM soliton. In principle, given the FDM particle mass, the profile of FDM soliton is fixed. In practice, however, there is a great diversity of structures in the Universe. In this paper, we enumerate some possible causes of such diversity, such as the effects of the gravitoelectric field, the gravitomagnetic field, an extra denser and compact FDM soliton and an ellipsoidal baryon background. And we find that the effects of the gravitomagnetic field are very weak but the effects of the others are considerable.

I. INTRODUCTION

The existence of dark matter (DM) can be inferred from the rotation curves of galaxies [1], the evolution of large scale structure [2] and the gravitational lensing observations [3]. According to the free streaming length of DM, DM can be divided into cold, warm and hot categories. Although the standard Lambda cold DM (Λ CDM) cosmological model is very successful and the latest cosmic microwave background (CMB) observations [4] suggests that CDM accounts for about 26% of today's energy density in the Universe, we don't know what particle or object CDM is. Especially, as one of the most promising candidates for CDM particle, the weak interacting massive particles (WIMPs) grounded on supersymmetric theories of particle physics still have not been detected [5–9]. Moreover, primordial black holes (BHs) can also serve as CDM [10] but they still have not been identified. These null results coupled with the failure of CDM particles on sub-galactic scales [11] imply that DM may not be cold.

There is a promising alternative to CDM which is an ultralight scalar field with spin-0, extraordinarily light mass ($\sim 10^{-22}$ eV/ c^2) and de Broglie wavelength comparable to few kpc, namely fuzzy DM (FDM) [12]. Due to the large occupation numbers in galactic halos, FDM behaves as a classical field obeying the coupled Schrödinger–Poisson (SP) system of equations

$$\begin{cases} i\hbar \frac{\partial \Psi}{\partial t} = \left(-\frac{\hbar^2}{2m} \nabla^2 + m\Phi \right) \Psi, \\ \nabla^2 \Phi = 4\pi G |\Psi|^2, \end{cases} \quad (1)$$

where m is the mass of FDM which is described by the wavefunction Ψ , the gravitational potential Φ is sourced by the FDM density $\rho = |\Psi|^2$. The SP system also

can govern the evolution of FDM in an expanding Universe [13–16]. It is worth noting that the SP system is just the weak field limit of the general relativistic Einstein–Klein–Gordon (EKG) system [17–19] and the SP system should be replaced by the Gross-Pitaevskii-Poisson (GPP) system when the self-interactions between FDM particles exist [20, 21].

For simplicity, in this paper, we confine ourself to the SP system in a non-expanding Universe. The evolution of this system is usually simulated numerically, including the formation, the perturbation, the interference/collision and the tidal disruption/deformation of FDM solitons [22–25]. If one just care about stationary solutions, one can turn to the shooting method to find the eigenvalues of equilibrium configurations [22, 26].

Since FDM solitons are only dependent on the mass of FDM, the SP system has the scaling symmetry. As a result, the Universe should be very monotonous and full of similar structures. But in fact there is a great diversity of structures in the Universe. Therefore, the real astrophysics systems must follow the different variants of the exact SP system, even though the modified gravity and the different interactions between FDM are not considered. In this paper, we will consider several variants due to different extra terms, such as the gravitoelectric field, the gravitomagnetic field, an extra FDM soliton and the baryon profile. Our motivations are as follows. First, as pointed out in [22], the SP system is the weak field limit of the EKG system. Therefore, there must be a variant system between these two ends where the gravitoelectromagnetism is a good approximation. While the gravitoelectric field or the gravitational potential of a super-massive BH has been discussed [24–26], the gravitomagnetic field due to the system's angular momentum has not been considered before. Secondly, although the interference/collision with an extra FDM soliton also has been studied [23–25], they just dealt with the cases where the density-ratio of two solitons is ~ 1 . For the extreme cases where the density-ratio of the denser solitons to another one is $\gtrsim 10^4$, numerical simulations need a larger simula-

*Corresponding author: wangkey@lzu.edu.cn

tion box to contain the larger soliton with lower density or need a higher resolution to depict the smaller soliton with higher density. However, a simulation with a larger simulation box and higher resolution at the same time is prohibitively expensive and almost impossible. Finally, a non-spherical baryon profile is located in galaxies which results in non-spherical FDM solitons, for example the impact of a baryon profile with the cylindrical symmetry and the parity symmetry has been quantified [27]. In fact, the baryon profile in the Milky Way may be ellipsoidal [28, 29].

This paper is organized as follows. In section II, we briefly review the effects of the gravitoelectric field due to a supermassive BH on the FDM solitons. In section III, we prove the effects of the gravitomagnetic field due to the rotation velocity of FDM, the supermassive black hole spin and the orbital motion of supermassive BH binary on the FDM solitons are negligible. In section IV, we study the interaction between soliton binary with the extreme density-ratio. In section V, we calculate the FDM solitons in a given ellipsoidal baryon profile. Finally, a brief summary and discussions are included in section VI.

II. EFFECTS OF THE GRAVITOELECTRIC FIELD

The effects of the gravitoelectric field includes the tidal disruption/deformation of FDM solitons by a nearby supermassive BH [24, 25] and the modified formation of FDM solitons by a central supermassive BH [26]. While the former non-spherical impacts are more complicated and have to be studied by numerical simulations, the latter spherical ones are simple and can be studied by the shooting method. In this section, we briefly review the latter cases.

Firstly, the gravitoelectric field \mathbf{E}_g or the gravitational potential Φ_e sourced by a central supermassive BH contributes to a variant of the exact SP system as

$$\begin{cases} i\hbar \frac{\partial \Psi}{\partial t} = \left[-\frac{\hbar^2}{2m} \nabla^2 + m(\Phi + \Phi_e) \right] \Psi, \\ \nabla^2 \Phi = 4\pi G |\Psi|^2, \end{cases} \quad (2)$$

where the supermassive BH with mass M_{bh} has a point mass potential

$$\Phi_e = -\frac{GM_{\text{bh}}}{r}. \quad (3)$$

When the system in question features the spherical symmetry, the ansatz of $\Psi(r, t) = e^{-i\gamma t/\hbar} \psi(r)$ means the FDM soliton density is $\rho(r) = |\Psi|^2 = \psi^2(r)$ and the FDM soliton mass is $M = \int_0^\infty 4\pi r^2 \rho(r) dr$. After defin-

ing a number of dimensionless variables as

$$\tilde{\psi} \equiv \frac{\hbar\sqrt{4\pi G}}{mc^2} \psi, \quad (4)$$

$$\tilde{r} \equiv \frac{mc}{\hbar} r, \quad (5)$$

$$\tilde{\Phi} \equiv \frac{1}{c^2} \Phi, \quad (6)$$

$$\tilde{\gamma} \equiv \frac{1}{mc^2} \gamma, \quad (7)$$

$$\tilde{M} \equiv \frac{GMm}{\hbar c}, \quad (8)$$

$$\tilde{M}_{\text{bh}} \equiv \frac{GM_{\text{bh}}m}{\hbar c}, \quad (9)$$

the dimensionless version of Eq. (2) is

$$\begin{cases} \frac{\partial^2(\tilde{r}\tilde{\psi})}{\partial \tilde{r}^2} = 2\tilde{r} \left(\tilde{\Phi} - \tilde{\gamma} - \frac{\tilde{M}_{\text{bh}}}{\tilde{r}} \right) \tilde{\psi}, \\ \frac{\partial^2(\tilde{r}\tilde{\Phi})}{\partial \tilde{r}^2} = \tilde{r}\tilde{\psi}^2. \end{cases} \quad (10)$$

Fulfilling the arbitrary normalization $\tilde{\psi}(\tilde{r} = 0) = 1$ and $\tilde{\Phi}(\tilde{r} = 0) = 0^1$, the boundary conditions $\tilde{\psi}(\tilde{r} = \infty) = 0$, $\frac{\partial \tilde{\psi}}{\partial \tilde{r}}|_{\tilde{r}=0} = 0$ and $\frac{\partial \tilde{\Phi}}{\partial \tilde{r}}|_{\tilde{r}=0} = 0$, choosing the supermassive BH mass $\tilde{M}_{\text{bh}} = \{0.0, 0.5, 1.0, 1.5, 2.0, 2.5\}$ as the input parameter and adjusting the quantized eigenvalue $\tilde{\gamma}$, we can calculate the equilibrium configurations from Eq. (10) by the shooting method. Given the input parameter \tilde{M}_{bh} , only the solution from the smallest $\tilde{\gamma}$ is stable and the ground state. In Tab. I, we list the input values of \tilde{M}_{bh} and the corresponding eigenvalue $\tilde{\gamma}$ and soliton mass \tilde{M} of the ground state solutions. In Fig. 1, the corresponding soliton profiles are plotted. We find that the larger \tilde{M}_{bh} leads to a more denser and compact soliton, hence a smaller dimensionless soliton mass \tilde{M} due to the fixed normalization $\tilde{\psi}(\tilde{r} = 0) = 1$. As for its physical mass M , in fact it increases with \tilde{M}_{bh} .

¹ Although the normalization $\tilde{\Phi}(\tilde{r} = 0) = 0$ for Φ is different from the normalization $\Phi_e(r = \infty) = 0$ for Φ_e (Eq. (3)), this difference does not affect the solutions with the normalization $\tilde{\psi}(\tilde{r} = 0) = 1$.

TABLE I: Input values of the supermassive BH mass \tilde{M}_{bh} and the corresponding eigenvalue $\tilde{\gamma}$ and soliton mass \tilde{M} of the ground state solutions.

\tilde{M}_{bh}	$\tilde{\gamma}$	\tilde{M}
0.0	0.6495	2.0622
0.5	0.1164	0.7916
1.0	-0.5113	0.2169
1.5	-1.0839	0.0718
2.0	-1.9767	0.0309
2.5	-3.1101	0.0159

III. EFFECTS OF THE GRAVITOMAGNETIC FIELD

The SP system is the weak field limit of the general relativistic EKG system [22]. Therefore, there must be a variant system between these two extreme ends by taking some general relativistic corrections into consideration, for example the gravitomagnetic field \mathbf{B}_g . Then there is a variant of the exact SP system as

$$\begin{cases} i\hbar \frac{\partial \Psi}{\partial t} = \left[-\frac{\hbar^2}{2m} \nabla^2 + m(\Phi + \Phi_e + \Phi_m) \right] \Psi, \\ \nabla^2 \Phi = 4\pi G |\Psi|^2, \end{cases} \quad (11)$$

where the gravitational potential Φ_m is related to the gravitomagnetic field \mathbf{B}_g and the angular momentum of FDM particle $\hat{\mathbf{L}}$ as

$$\begin{aligned} \Phi_m &= \Phi_{m1} + \Phi_{m2} \\ &= -\frac{1}{2m} \mathbf{B}_g \cdot \hat{\mathbf{L}} + \frac{1}{8} [(\mathbf{r} \cdot \mathbf{r})(\mathbf{B}_g \cdot \mathbf{B}_g) - (\mathbf{r} \cdot \mathbf{B}_g)(\mathbf{r} \cdot \mathbf{B}_g)]. \end{aligned} \quad (12)$$

Generally speaking, the linear term Φ_{m1} is much larger than the quadratic one Φ_{m2} . In this section, we will talk about some possible sources of \mathbf{B}_g and their effects on the FDM solitons.

A. Gravitomagnetic field due to rotation velocity of fuzzy dark matter

The gravitational potential inside a FDM soliton sourced by its own density profile is

$$\Phi = -\frac{4\pi G \int_0^r \rho(R) R^2 dR}{r} - 4\pi G \int_r^\infty \frac{\rho(R) R^2 dR}{R}, \quad (13)$$

where we temporarily utilize the normalization $\Phi(r = \infty) = 0$ in this subsection. If this FDM soliton is rotating around the z -axis, there should be a gravitomagnetic field \mathbf{B}_g according to the gravitoelectromagnetism. To calculate the total \mathbf{B}_g inside the FDM soliton, we first

consider a FDM shell with radius R rotating around the z -axis with a typical linear velocity relative to the FDM soliton's center $v \sim 10^{-3}c$. The magnitude of the gravitomagnetic field in the $x-y$ plane produced by this FDM shell is

$$dB_g = \begin{cases} \frac{4\pi G v \rho(R) R^3 dR}{3c^2 r^3}, & (r > R), \\ -\frac{8\pi G}{3c^2} v \rho(R) dR, & (r < R). \end{cases} \quad (14)$$

Then the magnitude of the gravitomagnetic field in the $x-y$ plane produced by the whole FDM soliton is

$$\begin{aligned} B_g &= \frac{4\pi G v}{3c^2} \left(\frac{1}{r^3} \int_0^r \rho(R) R^3 dR - 2 \int_r^\infty \rho(R) dR \right) \\ &= \frac{4\pi G v}{3c^2} f(r). \end{aligned} \quad (15)$$

There is an analytic fit to the soliton density from [13]

$$\rho(r) \approx \frac{0.019 \times (m/10^{-22} \text{eV}/c^2)^{-2} (r_c/\text{kpc})^{-4}}{[1 + 0.091 \times (r/r_c)^2]^8} M_\odot \text{pc}^{-3}, \quad (16)$$

where r_c is the radius of the soliton

$$M \times r_c \approx 2.2 \times 10^8 (m/10^{-22} \text{eV}/c^2)^{-2} M_\odot \text{kpc}. \quad (17)$$

and the soliton mass M can be predicted from the halo mass M_{halo} according to the soliton-halo mass relation [14]

$$M \approx 1.25 \times 10^9 \left(\frac{M_{\text{halo}}}{10^{12} M_\odot} \right)^{1/3} \left(\frac{m}{10^{-22} \text{eV}/c^2} \right)^{-1} M_\odot. \quad (18)$$

For a FDM particle rotating in the $x-y$ plane, the magnitude of its angular momentum is $L = mvr$, where its linear velocity relative to the FDM soliton's center is typically $v \sim 10^{-3}c$. According to Eq. (12), the linear gravitational potential in the $x-y$ plane is

$$\Phi_{m1} = -\frac{1}{2m} B_g L = -\frac{2\pi \times 10^{-6}}{3} G f(r) r, \quad (19)$$

and the quadratic gravitational potential in the $x-y$ plane is

$$\Phi_{m2} = \frac{1}{8} B_g^2 r^2 = \frac{2\pi^2 \times 10^{-6}}{9} \frac{G^2}{c^2} f(r)^2 r^2. \quad (20)$$

The gravitational potentials Φ (Eq. (13)), Φ_{m1} (Eq. (19)) and Φ_{m2} (Eq. (20)) include some complicated integrals so it's not easy to compare them directly. For clarity, we plot the gravitational potentials of $|\Phi|$, $|\Phi_{m1}|$ and $|\Phi_{m2}|$ in the $x-y$ plane in Fig. 2. We find Φ is dominant over Φ_{m1} and Φ_{m2} in the $x-y$ plane and the latter two can be neglected.

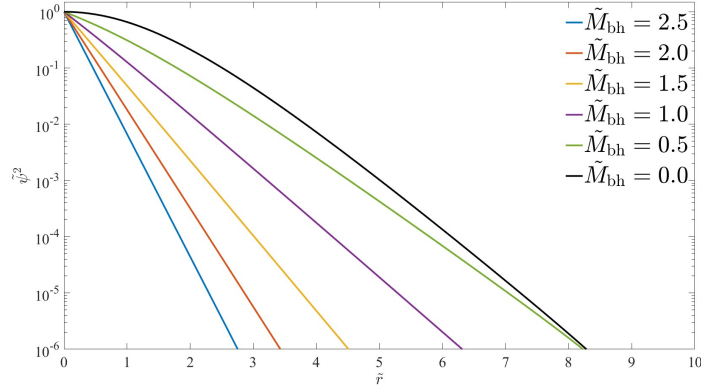


FIG. 1: The density profiles of the ground state solutions with different supermassive BH mass \tilde{M}_{bh} .

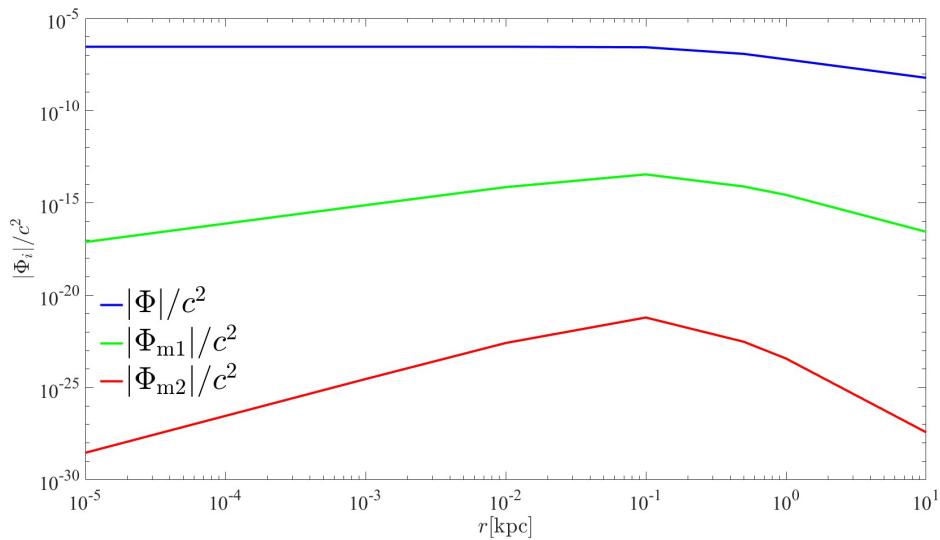


FIG. 2: The gravitational potentials of $|\Phi|$ (Eq. (13)), $|\Phi_{\text{m1}}|$ (Eq. (19)) and $|\Phi_{\text{m2}}|$ (Eq. (20)) in the $x - y$ plane, where the halo mass is similar to the Milky Way's $M_{\text{halo}} \approx 1 \times 10^{12} M_{\odot}$ [30] and the FDM particle has the typical mass $m = 10^{-22} \text{eV}/c^2$.

B. Gravitomagnetic field due to a supermassive black hole spin

Firstly we relate the Schwarzschild radius $R_S = \frac{2GM_{\text{bh}}}{c^2}$ to an arbitrary radial distance r as $r = nR_S$. For example, for the supermassive BH at the center of the Milky Way, its mass is $M_{\text{bh}} \approx 4 \times 10^6 M_{\odot}$ and Schwarzschild radius is $R_S \approx 1.2 \times 10^{10} \text{m} \approx 4 \times 10^{-7} \text{pc}$. Then the gravitational potential sourced by a central supermassive BH is

$$\Phi_e = -\frac{GM_{\text{bh}}}{r} = -\frac{c^2}{2n}. \quad (21)$$

If this supermassive BH is spinning, the magnitude of its angular momentum is $L_{\text{bh}} = \chi \frac{GM_{\text{bh}}^2}{c}$, where χ is a dimensionless spin parameter.

According to the gravitoelectromagnetism, the gravitomagnetic field \mathbf{B}_g is dependent on the angular momentum \mathbf{L}_{bh} as

$$\mathbf{B}_g = \frac{G}{2c^2} \frac{\mathbf{L}_{\text{bh}} - 3(\mathbf{L}_{\text{bh}} \cdot \mathbf{r}/r)\mathbf{r}/r}{r^3}. \quad (22)$$

Therefore, the magnitude of the gravitomagnetic field due to this spinning massive BH in the $x - y$ plane is

$$B_g = \frac{G}{2c^2} \frac{L_{\text{bh}}}{r^3} = \frac{\chi}{8n^3} \frac{c}{R_S}. \quad (23)$$

For a FDM particle rotating in the $x - y$ plane, the magnitude of its angular momentum is $L = mvr$, where its linear velocity relative to the central supermassive BH

is typically $v \sim 10^{-3}c$. According to Eq. (12), the linear gravitational potential in the $x - y$ plane is

$$\Phi_{m1} = -\frac{1}{2m}B_g L \sim -\frac{\chi}{16n^2} \times 10^{-3}c^2, \quad (24)$$

and the quadratic gravitational potential in the $x - y$ plane is

$$\Phi_{m2} = \frac{1}{8}B_g^2 r^2 = \frac{\chi^2}{512n^4}c^2. \quad (25)$$

Comparing the gravitational potentials calculated by Eq. (21), Eq. (24) and Eq. (25), we find Φ_e is dominant over Φ_{m1} and Φ_{m2} in the $x - y$ plane and the latter two can be neglected for $n \geq 1$. For clarity, we plot the gravitational potentials of $|\Phi_e|$, $|\Phi_{m1}|$ and $|\Phi_{m2}|$ in the $x - y$ plane as a function of n in Fig. 3, where $n \geq 1$ means the radial distance is larger than the Schwarzschild radius of the supermassive BH. For these FDM particles not located in the $x - y$ plane or located in the $x - y$ plane but not rotating around the central supermassive BH, Φ_e is further dominant.

C. Gravitomagnetic field due to the orbital motion of a supermassive black hole binary

For simplicity, we consider a supermassive BH binary in a circular orbit in the $x - y$ plane. These two supermassive BHs share the same mass M_{bh} and have a separation $S = sR_S$ between each other, where s is a parameter. Then the magnitude of the angular momentum of this binary is

$$L_{\text{bbh}} = I_{\text{bbh}}\Omega_{\text{bbh}} = \sqrt{s}\frac{GM_{\text{bh}}^2}{c}, \quad (26)$$

where the moment of inertia of this binary is $I_{\text{bbh}} = \frac{1}{2}M_{\text{bh}}S^2$ and the angular frequency of this binary is $\Omega_{\text{bbh}} = \frac{1}{\sqrt{s}}\frac{c}{S}$. According to Eq. (22), the magnitude of the gravitomagnetic field due to this binary in the $x - y$ plane is

$$B_g = \frac{G}{2c^2}\frac{L_{\text{bbh}}}{r^3} = \frac{\sqrt{s}}{8n^3}\frac{c}{R_S}. \quad (27)$$

Also for a FDM particle rotating in the $x - y$ plane, the magnitude of its angular momentum is $L = mvr$, where its linear velocity relative to this binary is typically $v \sim 10^{-3}c$. According to Eq. (12), the linear gravitational potential in the $x - y$ plane is

$$\Phi_{m1} = -\frac{1}{2m}B_g L \sim -\frac{\sqrt{s}}{16n^2} \times 10^{-3}c^2, \quad (28)$$

and the quadratic gravitational potential in the $x - y$ plane is

$$\Phi_{m2} = \frac{1}{8}B_g^2 r^2 = \frac{s}{512n^4}c^2. \quad (29)$$

We plot the gravitational potentials of $|\Phi_e| = \frac{c^2}{n}$, $|\Phi_{m1}|$ (Eq. (28)) and $|\Phi_{m2}|$ (Eq. (29)) in the $x - y$ plane as a function of n in Fig. 4, where $n \geq 1 + \frac{s}{2}$ means the radial distance is larger than the Schwarzschild radius of each supermassive BH plus half separation $R_S + \frac{s}{2}$. We find Φ_e is dominant over Φ_{m1} and Φ_{m2} in the $x - y$ plane and the latter two can be neglected for $n \geq 1 + \frac{s}{2}$, let alone these FDM particles not located in the $x - y$ plane or located in the $x - y$ plane but not rotating around this binary.

IV. EFFECTS OF THE EXTREME DENSITY-RATIO OF SOLITON BINARY

For the cases where the density-ratio of two solitons is ~ 1 , this system obviously does not feature the spherical symmetry and can be studied by numerical simulations [23–25]. On the contrary, for the extreme case where the density-ratio of two solitons is $\gtrsim 10^4$, there are two stages when this system do feature an approximate and local spherical symmetry: stage 1) the smaller soliton with higher density is just immerse in the boundary of the larger soliton with lower density which is relatively flat and can be considered as a background; stage 2) the larger soliton with lower density shares the same center with the smaller soliton with higher density which are more stable and can be considered as a background. The collisional dynamics include these two stages and we can still use the shooting method to deal with them. Finally, we can use the exact SP system (Eq. (1)) to describe the background soliton and the following variant of the exact SP system to describe the changed soliton during the above two stages

$$\begin{cases} i\hbar\frac{\partial\Psi}{\partial t} = \left(-\frac{\hbar^2}{2m}\nabla^2 + m\Phi\right)\Psi, \\ \nabla^2\Phi = 4\pi G(|\Psi|^2 + \rho_{\text{bg}}), \end{cases} \quad (30)$$

whose dimensionless version is

$$\begin{cases} \frac{\partial^2(\tilde{r}\tilde{\psi})}{\partial\tilde{r}^2} = 2\tilde{r}(\tilde{\Phi} - \tilde{\gamma})\tilde{\psi}, \\ \frac{\partial^2(\tilde{r}\tilde{\Phi})}{\partial\tilde{r}^2} = \tilde{r}(\tilde{\psi}^2 + \tilde{\rho}_{\text{bg}}), \end{cases} \quad (31)$$

where ρ_{bg} is the density of the background soliton and its dimensionless counterpart is

$$\tilde{\rho}_{\text{bg}} \equiv \left(\frac{\hbar\sqrt{4\pi G}}{mc^2}\right)^2 \rho_{\text{bg}}. \quad (32)$$

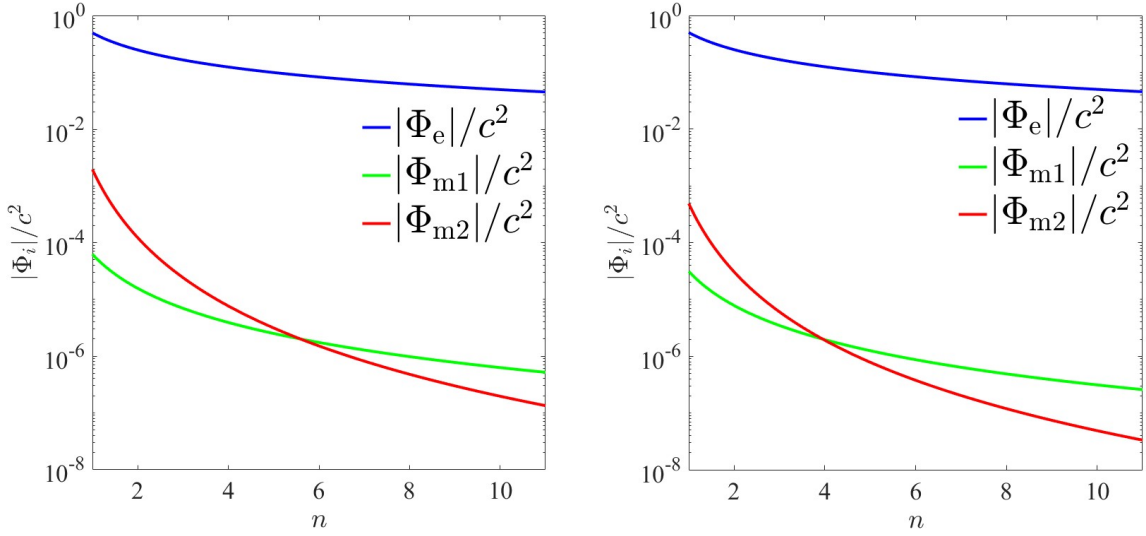


FIG. 3: The gravitational potentials of $|\Phi_e|$, $|\Phi_{m1}|$ and $|\Phi_{m2}|$ in the $x - y$ plane as a function of n calculated by Eq. (21), Eq. (24) and Eq. (25) respectively, where $n \geq 1$ means the radial distance is larger than the Schwarzschild radius of the supermassive BH. The left subplot is plotted with $\chi = 1$ and the right subplot is plotted with $\chi = 0.5$.

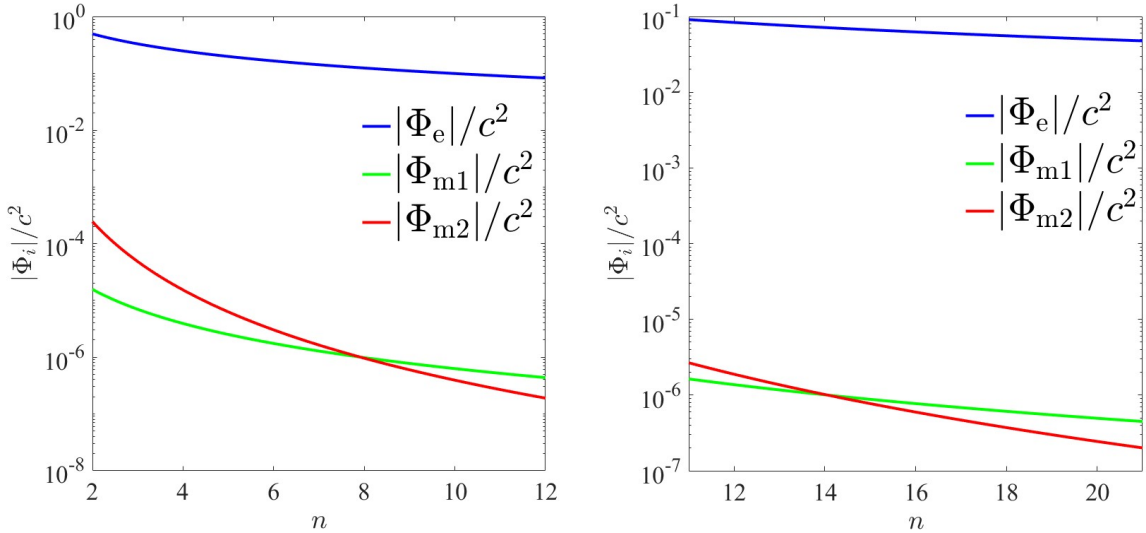


FIG. 4: The gravitational potentials of $|\Phi_e| = \frac{c^2}{n}$, $|\Phi_{m1}|$ (Eq. (28)) and $|\Phi_{m2}|$ (Eq. (29)) in the $x - y$ plane as a function of n , where $n \geq 1 + \frac{s}{2}$ means the radial distance is larger than the Schwarzschild radius of each supermassive BH plus half separation $R_S + \frac{S}{2}$. The left subplot is plotted with $s = 2$ and the right subplot is plotted with $s = 20$.

Since this variant SP system (Eq. (31)) has the scaling symmetry

$$\tilde{\psi} \longrightarrow \lambda \tilde{\psi}, \quad (33)$$

$$\tilde{r} \longrightarrow \lambda^{-1/2} \tilde{r}, \quad (34)$$

$$\tilde{\Phi} \longrightarrow \lambda \tilde{\Phi}, \quad (35)$$

$$\tilde{\gamma} \longrightarrow \lambda \tilde{\gamma}, \quad (36)$$

$$\tilde{M} \longrightarrow \lambda^{1/2} \tilde{M}, \quad (37)$$

$$\tilde{\rho}_{\text{bg}} \longrightarrow \lambda^2 \tilde{\rho}_{\text{bg}}, \quad (38)$$

we can set up the background soliton with $\lambda = 10^{-2}$ for stage 1 and with $\lambda = 10^2$ for stage 2. Given the background density ρ_{bg} , the changed soliton can be found by solving Eq. (31) with the shooting method. By assuming that its density profile $\tilde{\psi}^2(\tilde{r})$ is changing but its dimensionless mass \tilde{M} is fixed as the initial value listed in the first row of Tab. I, we get the eigenvalue $\tilde{\gamma} = 0.6495$ for stage 1 and the eigenvalue $\tilde{\gamma} = 69.2491$ for stage 2. For stage 1, the density profile $\tilde{\psi}^2(\tilde{r})$ of each soliton is shown in the left subplot of Fig. 5; for stage 2, each soliton's $\tilde{\psi}^2(\tilde{r})$ is shown in the right subplot of Fig. 5. We can find that the smaller soliton with higher density is almost not affected by the background soliton for stage 1 and the larger soliton with lower density shrink dramatically for stage 2. After stage 2, there are two comparable solitons and the system becomes complicated whose further evolution should be studied by numerical simulation.

V. EFFECTS OF THE ELLIPSOIDAL BARYON PROFILE

Instead of a background soliton shown in section IV, we consider a background baryon profile in this section. More precisely, we consider an ellipsoidal baryon profile similar to the Milk Way's [28, 29]

$$\rho_{\text{bg}}(x, y, z) = \rho_{\text{bulge}}(x, y, z) + \rho_{\text{disk}}(x, y, z) + \rho_{\text{gas}}(x, y, z), \quad (39)$$

where ρ_{bulge} is a triaxial and bar-shaped bulge of stars at the inner few kpc of the Milky Way [31, 32]

$$\rho_{\text{bulge}}(x, y, z) = 9.9 M_{\odot} \text{pc}^{-3} \times \exp \left\{ - \left[x^2 + \left(\frac{y}{0.49} \right)^2 + \left(\frac{z}{0.37} \right)^2 \right]^{1/2} / 740 \text{pc} \right\}, \quad (40)$$

the disk density $\rho_{\text{disk}} \approx 0.05 M_{\odot} \text{pc}^{-3}$ [31] can be neglected but ρ_{gas} is a non-negligible part of the baryons in the Milky Way in the form of molecular, atomic and ionised hydrogen and heavier elements. Here we assume that $\rho_{\text{gas}} \approx m_{H_2} \langle n_{H_2} \rangle$, where m_{H_2} is the mass of molecular hydrogen and $\langle n_{H_2} \rangle$ is the number density of molec-

ular hydrogen in central molecular zone [33],

$$\langle n_{H_2} \rangle = 150 \text{cm}^{-3} \times \exp \left\{ - \left[\frac{\sqrt{x^2 + (2.5y)^2} - 125 \text{pc}}{137 \text{pc}} \right]^4 \times \exp \left[- \left(\frac{z}{18 \text{pc}} \right)^2 \right] \right\}. \quad (41)$$

For this non-spherical system, the shoot method is failed and numerical simulations should be performed. As an approximation, however, we consider three background baryon profiles respectively: $\rho_{\text{bg}}^x(r) = \rho_{\text{bg}}(x = r, y = 0, z = 0)$, $\rho_{\text{bg}}^y(r) = \rho_{\text{bg}}(x = 0, y = r, z = 0)$ and $\rho_{\text{bg}}^z(r) = \rho_{\text{bg}}(x = 0, y = 0, z = r)$. Then the shoot method still works for $\rho_{\text{bg}}^i(r)$. If the results by different $\rho_{\text{bg}}^i(r)$ are very different, it means the original $\rho_{\text{bg}}(x, y, z)$ is too non-spherical to be described by the approximation $\rho_{\text{bg}}^i(r)$.

To find the equilibrium configurations, as shown in section II, we usually use the arbitrary normalization $\tilde{\psi}(\tilde{r} = 0) = 1$. It means that the normalized soliton mass $\tilde{M} = \int_0^{\infty} \tilde{r}^2 \tilde{\psi}^2 d\tilde{r}$ is deviate from the true dimensionless mass by a scaling factor λ . For the Milk Way, the soliton physical mass $M \approx 1.25 \times 10^9 M_{\odot}$ is obtained with the soliton-halo mass relation [14]. On the other hand, taking this scaling factor into consideration, $\tilde{\rho}_{\text{bg}}^i \rightarrow \lambda^2 \tilde{\rho}_{\text{bg}}^i$ means the background baryon profile is modified. To fix both of the soliton mass and the background baryon profile as the Milk Way's, we introduce a scaling factor in advance and obtain a new dimensionless variant as

$$\begin{cases} \frac{\partial^2(\tilde{r}\tilde{\psi})}{\partial \tilde{r}^2} = 2\tilde{r}(\tilde{\Phi} - \tilde{\gamma})\tilde{\psi}, \\ \frac{\partial^2(\tilde{r}\tilde{\Phi})}{\partial \tilde{r}^2} = \tilde{r}(\tilde{\psi}^2 + \lambda_0^{-2} \tilde{\rho}_{\text{bg}}^i), \end{cases} \quad (42)$$

where λ_0^{-2} is a parameter and not changing with the scaling factor λ . Therefore, this system still has the scaling symmetry with $\lambda_0^{-2} \tilde{\rho}_{\text{bg}}^i \rightarrow \lambda^2 \lambda_0^{-2} \tilde{\rho}_{\text{bg}}^i$. Given an initial λ_0 , we can obtain the normalized soliton profile $\tilde{\psi}^2$. And then we can obtain the scaling factor λ by requiring the soliton mass to be the Milk Way's. If $\lambda/\lambda_0 \neq 1$, we replace the initial λ_0 with the newest λ and repeat the former two steps. When $\lambda/\lambda_0 - 1 < 0.0001$, we stop the iteration.

In Tab. II, Tab. III and Tab. IV, we list the eigenvalues $\tilde{\gamma}$, the soliton mass \tilde{M} of the ground state solutions and the final values of λ_0 for the different background baryon profile $\tilde{\rho}_{\text{bg}}^i$ and the mass of FDM m respectively. Meanwhile, we plot the normalized and the physical density profiles of the ground state solutions with different background baryon profile $\tilde{\rho}_{\text{bg}}^i$ and the mass of FDM m in Fig. 6. Comparing the soliton profiles with different $\tilde{\rho}_{\text{bg}}^i$ plotted in every subplot, we find the fine-structure of the background baryon profile does not matter and our treatment for the ellipsoidal baryon profile is reasonable. And again, comparing the soliton profiles with different m , we find the heavier FDM particles form a more compact denser soliton which is more insensitive to the background baryon profile.

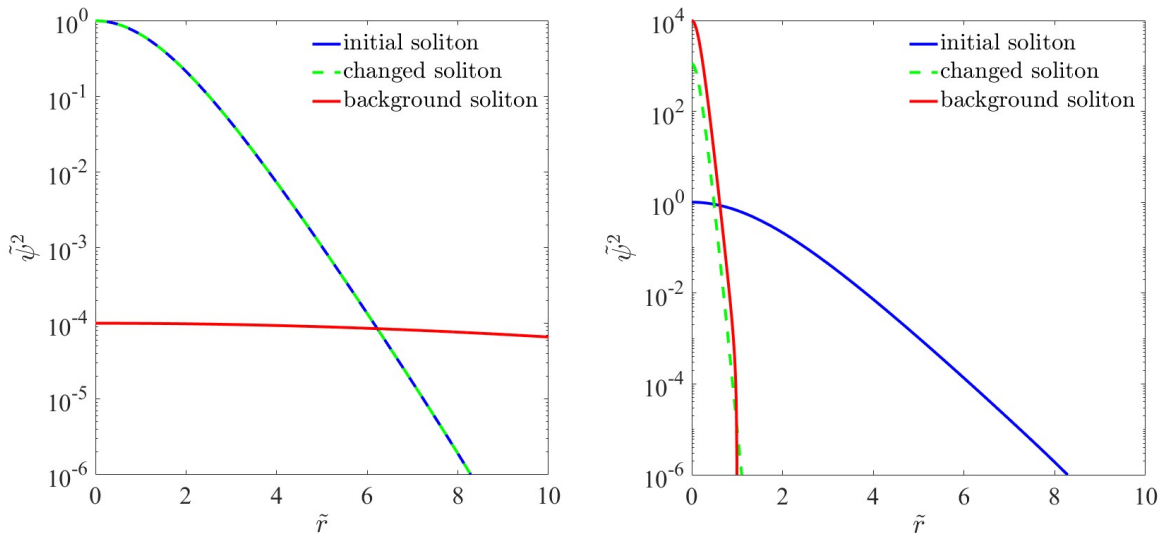


FIG. 5: The density profile $\tilde{\psi}^2(\tilde{r})$ of each soliton for stage 1 (left) and stage 2 (right).

TABLE II: Given the background baryon profile $\tilde{\rho}_{\text{bg}}^x$ and the mass of FDM m , the corresponding eigenvalue $\tilde{\gamma}$ and soliton mass \tilde{M} of the ground state solutions as well as the final values of λ_0 .

m	$\tilde{\gamma}$	\tilde{M}	λ_0
$1 \times 10^{-22} \text{eV}/c^2$	0.7600	1.4807	4.3088×10^{-7}
$2 \times 10^{-22} \text{eV}/c^2$	0.7037	1.7103	3.2300×10^{-7}
$5 \times 10^{-22} \text{eV}/c^2$	0.6644	1.9471	2.4920×10^{-7}

TABLE III: Given the background baryon profile $\tilde{\rho}_{\text{bg}}^y$ and the mass of FDM m , the corresponding eigenvalue $\tilde{\gamma}$ and soliton mass \tilde{M} of the ground state solutions as well as the final values of λ_0 .

m	$\tilde{\gamma}$	\tilde{M}	λ_0
$1 \times 10^{-22} \text{eV}/c^2$	0.7521	1.6009	3.6863×10^{-7}
$2 \times 10^{-22} \text{eV}/c^2$	0.7022	1.7670	3.0256×10^{-7}
$5 \times 10^{-22} \text{eV}/c^2$	0.6642	1.9483	2.4889×10^{-7}

VI. SUMMARY AND DISCUSSION

In this paper, we enumerate some reasonable variants of the exact SP system, such as the variants due to a central supermassive BH (section II), the system's own angular momentum (section III), an extra denser and com-

TABLE IV: Given the background baryon profile $\tilde{\rho}_{\text{bg}}^z$ and the mass of FDM m , the corresponding eigenvalue $\tilde{\gamma}$ and soliton mass \tilde{M} of the ground state solutions as well as the final values of λ_0 .

m	$\tilde{\gamma}$	\tilde{M}	λ_0
$1 \times 10^{-22} \text{eV}/c^2$	0.7265	1.6652	3.4068×10^{-7}
$2 \times 10^{-22} \text{eV}/c^2$	0.6859	1.8400	2.7970×10^{-7}
$5 \times 10^{-22} \text{eV}/c^2$	0.6596	1.9922	2.3805×10^{-7}

compact soliton (section IV) and an ellipsoidal baryon background (section V). All of them can be considered as an almost spherical system and solved with the shooting method. We reach the same conclusion [26] that the larger central supermassive BH makes the soliton more denser and compact. For the first time, we prove the gravitomagnetic field derived from the angular momentum can be neglected compared to the contributions from the gravitoelectric field which is the only survival in the Newtonian regime. Unlike the interference or collision of two similar solitons, the beginning of the interaction between two solitons with an extreme density-ratio is relatively simple: the smaller soliton with higher density is almost not affected but the larger soliton with lower density shrink dramatically. Finally, we revisit the topic discussed in [27] that the baryon background is important for the soliton profile. But we propose a reasonable treatment for the ellipsoidal baryon background and then

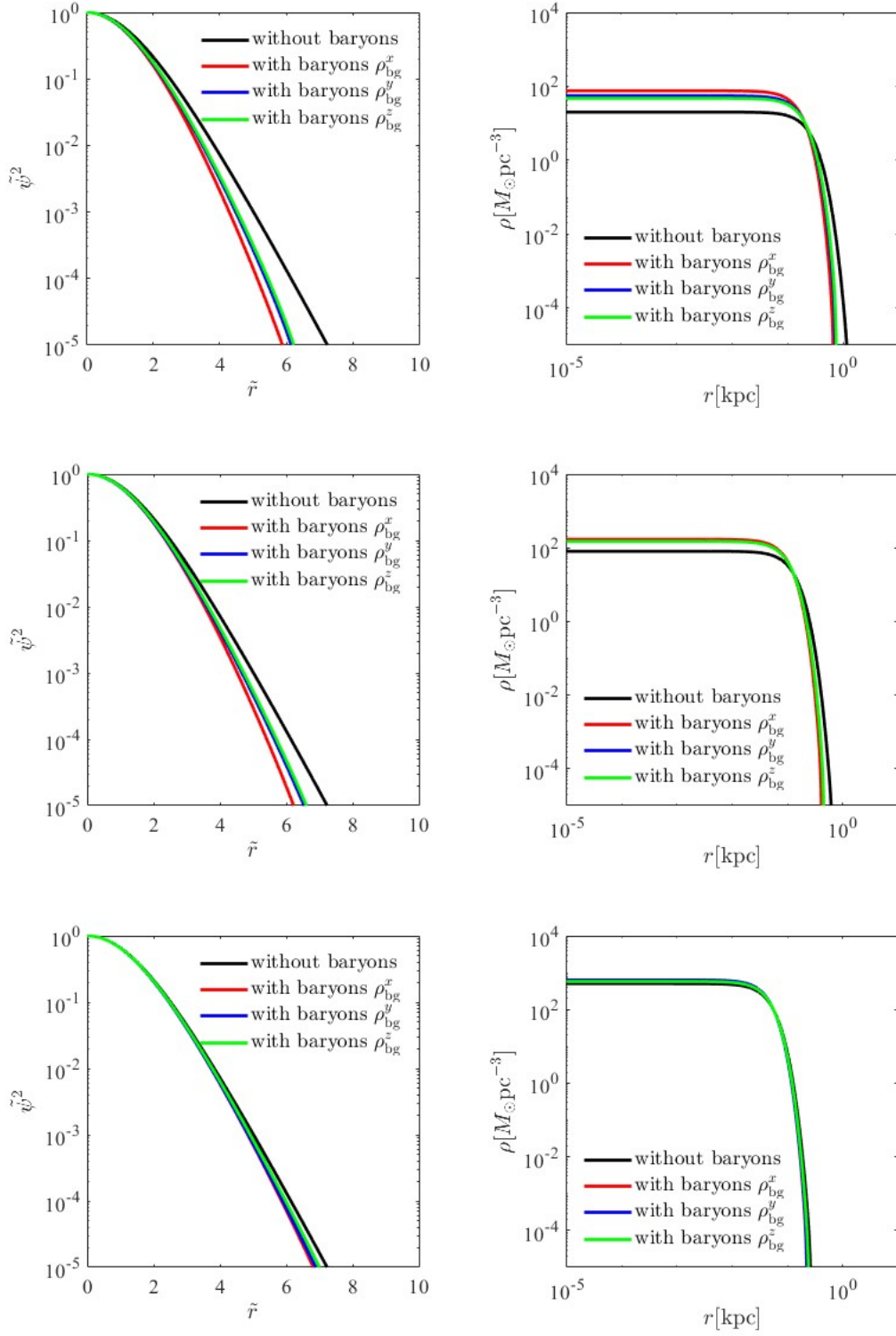


FIG. 6: The density profiles of the ground state solutions with different background baryon profile $\tilde{\rho}_{\text{bg}}^i$ and the mass of FDM m : the first row is plotted with $m = 1 \times 10^{-22} \text{eV}/c^2$, the second row is plotted with $m = 2 \times 10^{-22} \text{eV}/c^2$ and the third row is plotted with $m = 5 \times 10^{-22} \text{eV}/c^2$; the first column is the normalized density profile and the second column is the physical density profile; the black curves is plotted without the background baryon profile, the red curves is plotted with $\tilde{\rho}_{\text{bg}}^x$, the blue curves is plotted with $\tilde{\rho}_{\text{bg}}^y$ and the green curves is plotted with $\tilde{\rho}_{\text{bg}}^z$.

highlight the importance of the baryon background for lighter FDM particle.

Of course, we can enlarge the parameter space of the underlying theoretical model and produce a greater diversity in the solution of soliton. For example, the self-interactions between FDM particles [34] or the modified gravitational potential due to the modified gravity [35] would result in a different coupled equations, hence a different soliton profile. Although the Universe has picked out the only underlying rule, these variants of the exact

SP system presented in this paper are common to the theoretical models.

Acknowledgments

Ke Wang is supported by grants from NSFC (grant No.12247101).

-
- [1] V. C. Rubin, W. K. Ford, Jr., N. Thonnard and D. Burstein, “Rotational properties of 23 SB galaxies,” *Astrophys. J.* **261**, 439 (1982)
- [2] M. Davis, G. Efstathiou, C. S. Frenk and S. D. M. White, “The Evolution of Large Scale Structure in a Universe Dominated by Cold Dark Matter,” *Astrophys. J.* **292**, 371-394 (1985)
- [3] D. Clowe, M. Bradac, A. H. Gonzalez, M. Markevitch, S. W. Randall, C. Jones and D. Zaritsky, “A direct empirical proof of the existence of dark matter,” *Astrophys. J. Lett.* **648**, L109-L113 (2006) [arXiv:astro-ph/0608407 [astro-ph]].
- [4] N. Aghanim *et al.* [Planck], “Planck 2018 results. VI. Cosmological parameters,” *Astron. Astrophys.* **641**, A6 (2020) [erratum: *Astron. Astrophys.* **652**, C4 (2021)] [arXiv:1807.06209 [astro-ph.CO]].
- [5] A. Tan *et al.* [PandaX-II], “Dark Matter Results from First 98.7 Days of Data from the PandaX-II Experiment,” *Phys. Rev. Lett.* **117**, no.12, 121303 (2016) [arXiv:1607.07400 [hep-ex]].
- [6] D. S. Akerib *et al.* [LUX], “Improved Limits on Scattering of Weakly Interacting Massive Particles from Reanalysis of 2013 LUX Data,” *Phys. Rev. Lett.* **116**, no.16, 161301 (2016) [arXiv:1512.03506 [astro-ph.CO]].
- [7] “ATLAS Collaboration and CMS Collaboration (ATLAS, CMS) (2016).”
- [8] L. Accardo *et al.* [AMS], “High Statistics Measurement of the Positron Fraction in Primary Cosmic Rays of 0.5–500 GeV with the Alpha Magnetic Spectrometer on the International Space Station,” *Phys. Rev. Lett.* **113**, 121101 (2014)
- [9] M. Ackermann *et al.* [Fermi-LAT], “Measurement of separate cosmic-ray electron and positron spectra with the Fermi Large Area Telescope,” *Phys. Rev. Lett.* **108**, 011103 (2012) [arXiv:1109.0521 [astro-ph.HE]].
- [10] B. Carr, F. Kuhnel and M. Sandstad, “Primordial Black Holes as Dark Matter,” *Phys. Rev. D* **94**, no.8, 083504 (2016) [arXiv:1607.06077 [astro-ph.CO]].
- [11] J. Primack, “Cosmology: small scale issues revisited,” *New J. Phys.* **11**, 105029 (2009) [arXiv:0909.2247 [astro-ph.CO]].
- [12] W. Hu, R. Barkana and A. Gruzinov, “Cold and fuzzy dark matter,” *Phys. Rev. Lett.* **85**, 1158-1161 (2000) [arXiv:astro-ph/0003365 [astro-ph]].
- [13] H. Y. Schive, T. Chiueh and T. Broadhurst, “Cosmic Structure as the Quantum Interference of a Coherent Dark Wave,” *Nature Phys.* **10**, 496-499 (2014) [arXiv:1406.6586 [astro-ph.GA]].
- [14] H. Y. Schive, M. H. Liao, T. P. Woo, S. K. Wong, T. Chiueh, T. Broadhurst and W. Y. P. Hwang, “Understanding the Core-Halo Relation of Quantum Wave Dark Matter from 3D Simulations,” *Phys. Rev. Lett.* **113**, no.26, 261302 (2014) [arXiv:1407.7762 [astro-ph.GA]].
- [15] I. De Martino, T. Broadhurst, S. H. Henry Tye, T. Chiueh, H. Y. Schive and R. Lazkoz, “Recognizing Axionic Dark Matter by Compton and de Broglie Scale Modulation of Pulsar Timing,” *Phys. Rev. Lett.* **119**, no.22, 221103 (2017) [arXiv:1705.04367 [astro-ph.CO]].
- [16] P. Mocz, A. Fialkov, M. Vogelsberger, F. Becerra, M. A. Amin, S. Bose, M. Boylan-Kolchin, P. H. Chavanis, L. Hernquist and L. Lancaster, *et al.* “First star-forming structures in fuzzy cosmic filaments,” *Phys. Rev. Lett.* **123**, no.14, 141301 (2019) [arXiv:1910.01653 [astro-ph.GA]].
- [17] D. J. Kaup, “Klein-Gordon Geon,” *Phys. Rev.* **172** (1968), 1331-1342
- [18] R. Ruffini and S. Bonazzola, “Systems of self-gravitating particles in general relativity and the concept of an equation of state,” *Phys. Rev.* **187** (1969), 1767-1783
- [19] T. X. Ma, C. Liang, J. Yang and Y. Q. Wang, “Hybrid Proca-boson stars,” *Phys. Rev. D* **108**, no.10, 104011 (2023) [arXiv:2304.08019 [gr-qc]].
- [20] P. H. Chavanis, “Mass-radius relation of Newtonian self-gravitating Bose-Einstein condensates with short-range interactions: I. Analytical results,” *Phys. Rev. D* **84**, 043531 (2011) [arXiv:1103.2050 [astro-ph.CO]].
- [21] P. H. Chavanis and L. Delfini, “Mass-radius relation of Newtonian self-gravitating Bose-Einstein condensates with short-range interactions: II. Numerical results,” *Phys. Rev. D* **84**, 043532 (2011) [arXiv:1103.2054 [astro-ph.CO]].
- [22] F. S. Guzman and L. A. Urena-Lopez, “Evolution of the Schrodinger-Newton system for a selfgravitating scalar field,” *Phys. Rev. D* **69**, 124033 (2004) [arXiv:gr-qc/0404014 [gr-qc]].
- [23] A. Paredes and H. Michinel, “Interference of Dark Matter Solitons and Galactic Offsets,” *Phys. Dark Univ.* **12**, 50-55 (2016) [arXiv:1512.05121 [astro-ph.CO]].
- [24] F. Edwards, E. Kendall, S. Hotchkiss and R. Easther, “PyUltraLight: A Pseudo-Spectral Solver for Ultralight Dark Matter Dynamics,” *JCAP* **10**, 027 (2018) [arXiv:1807.04037 [astro-ph.CO]].
- [25] E. Munive-Villa, J. N. Lopez-Sanchez, A. A. Avilez-Lopez and F. S. Guzman, “Solving the Schrödinger-Poisson system using the coordinate adaptive moving mesh method,” *Phys. Rev. D* **105**, no.8, 083521 (2022) [arXiv:2203.10234 [gr-qc]].
- [26] E. Y. Davies and P. Mocz, “Fuzzy Dark Matter Soli-

- ton Cores around Supermassive Black Holes,” *Mon. Not. Roy. Astron. Soc.* **492**, no.4, 5721-5729 (2020) [arXiv:1908.04790 [astro-ph.GA]].
- [27] N. Bar, K. Blum, J. Eby and R. Sato, “Ultralight dark matter in disk galaxies,” *Phys. Rev. D* **99**, no.10, 103020 (2019) [arXiv:1903.03402 [astro-ph.CO]].
- [28] F. Iocco, M. Pato and G. Bertone, “Evidence for dark matter in the inner Milky Way,” *Nature Phys.* **11**, 245-248 (2015) [arXiv:1502.03821 [astro-ph.GA]].
- [29] H. N. Lin and X. Li, “The Dark Matter Profiles in the Milky Way,” *Mon. Not. Roy. Astron. Soc.* **487**, no.4, 5679-5684 (2019) [arXiv:1906.08419 [astro-ph.GA]].
- [30] W. Wang, J. Han, M. Cautun, Z. Li and M. N. Ishigaki, “The mass of our Milky Way,” *Sci. China Phys. Mech. Astron.* **63**, no.10, 109801 (2020) [arXiv:1912.02599 [astro-ph.GA]].
- [31] M. Lopez-Corredoira, A. Cabrera-Lavers and O. E. Gerhard, “A Boxy bulge in the Milky Way. Inversion of the stellar statistics equation with 2MASS data,” *Astron. Astrophys.* **439**, 107 (2005) [arXiv:astro-ph/0504608 [astro-ph]].
- [32] Y. H. Ryu, H. Y. Chang, M. G. Park and K. W. Lee, “Microlensing Optical Depth Revisited with Recent Star Counts,” *Astrophys. J.* **689**, 1078 (2008) [arXiv:0808.2539 [astro-ph]].
- [33] K. Ferriere, W. Gillard and P. Jean, “Spatial distribution of interstellar gas in the innermost 3 kpc of our Galaxy,” *Astron. Astrophys.* **467**, 611-627 (2007) [arXiv:astro-ph/0702532 [astro-ph]].
- [34] P. H. Chavanis, “Mass-radius relation of self-gravitating Bose-Einstein condensates with a central black hole,” *Eur. Phys. J. Plus* **134**, no.7, 352 (2019) [arXiv:1909.04709 [gr-qc]].
- [35] J. Chen and H. Y. Zhang, “Novel structures and collapse of solitons in nonminimally gravitating dark matter halos,” *JCAP* **10**, 005 (2024) [arXiv:2407.09265 [hep-ph]].